J Mater Sci (2009) 44:2063–2068
DOI 10.1007/s10853-009-3300-7

Effect of green density and electric field direction on densification of YAG nano-powders by spark plasma sintering

O. Tobi Even-Zur · R. Chaim

Received: 13 November 2008 / Accepted: 26 January 2009 / Published online: 26 February 2009

Abstract Nanocrystalline YAG powders with 34-nm average particle size were cold isostatic pressed (CIP) between 10 and 240 MPa to form compacts with 43–52% green densities. Spark plasma sintering (SPS) was performed for 5 min at 1,400 °C and 90 MPa using clusters of three disc specimens packed in series with the electric field direction. The pore size and its volume fraction decreased with the increase in the CIP pressure. The final density varied between 86% and 99% and strongly depended on the specimen location in the series. Density, grain size, and pore size analyses showed that the specimens facing the electric current experienced higher SPS temperatures. Possible temperature gradient due to axial displacement of non-conducting oxide was too low to explain the observed effect. Effect of the green density on the final density was marginal.

Introduction

Spark plasma sintering (SPS) is a novel hot-pressing technique used for rapid densification of ceramic powders within a few minutes. It necessitates high heating rates from 300 to 600 °C/min which were achieved by application of high-density pulsed dc electric current at low voltages [1–3]. The advantage of the SPS technique is also attributed to its versatile nature, where both the powder and the process parameters can be controlled and affect the sintering and densification as well as other material processes [4–7]. Therefore, SPS has recently been used for the processing of many different materials and functionalities [8].

SPS provides the conditions for preservation of the nanocrystalline character during densification of ceramics [9–12]. However, it was shown that full densification necessitated diffusional processes in order to anneal out the closed pores at the grain boundaries. This in turn may lead to the loss of the nanocrystalline character by enhanced grain growth at the final stage of sintering [13]. In conventional sintering, wide pore size distribution as well as large pores in the green compact—compared to the particle size—may result in more stable residual pores due to differential shrinkage [14, 15]. Cold isostatic pressing (CIP) is used for reduction of the pore size in general and to homogenization of its distribution throughout the green specimen, in particular. Densification of YAG and Nd-YAG nanoparticles was recently investigated and the underlying densification mechanisms were revealed [16, 17]. This study investigated the effect of the green density on densification of YAG nano-powders. The experimental findings highlighted the effect of the electric field direction on the densification behavior.

Experimental procedure

Pure commercial YAG nano-powder (Nanocerox, U.S.A) with average particle diameter of 34 nm was used, the characteristics of which were given in detail elsewhere [16]. Large series of green compacts were prepared by uniaxial pressing of 1 g nano-powder at 17 MPa into discs of 12 mm in diameter and of 3.87-mm average thickness. The resultant green discs were further cold isostatic pressed (CIP) at different pressures between 10 and 240 MPa. The compact green density was determined by weighing.

O. T. Even-Zur · R. Chaim (✉)
Department of Materials Engineering, Technion-Israel Institute of Technology, Haifa 32000, Israel
e-mail: rchaim@technion.ac.il

Selected specimens differing in their CIP pressure were used for porosity tests using Mercury porosimeter (Macropore 120). The green compacts were fired in air at 800 °C for 2 h at the heating and cooling rates of 20 °C/min prior to the porosity test. This firing was accompanied by ~1% linear shrinkage; hence, it did not affect the porosity character; it formed necks between the nano-particles so that the skeletal integrity of the compact is preserved during the Hg intrusion and extrusion.

SPS experiments were performed using the SPS apparatus (FCT Systems GmbH, Germany). Each SPS run included three disc specimens located within a graphite die, separated from each other and from the die surface by graphite foils (Fig. 1). In this respect, the three specimens were packed and aligned in series with the SPS electric field. All the SPS runs were performed for 5 min at 1,400 °C and 90 MPa using the heating rate of 150 °C/min. The average current density was 550 A cm^{-2} at 4 V; the pulse and pause durations were 5 and 2 ms, respectively. Finally, the batch was cooled to room temperature at a rate of 117 °C/min during which the load was released simultaneously. The final density of the specimens was measured by the Archimedes method using distilled water as the immersion liquid; the relative density was calculated assuming a theoretical density 4.5533 g cm^{-3}. The specimens were numbered in order to follow their process history for comparison.

Scanning electron microscopy (SEM, LEO Gemini 982) operated at 4 kV was used for microstructure characterization of the dense specimens. SEM specimens were prepared by mechanical polishing down to 1 μm, followed by thermal etching at 1,180 °C for 30 min and carbon coating. The grain size and its distribution were determined by image analysis using Scion image (NIH), where more than 400 grains were counted for each specimen.

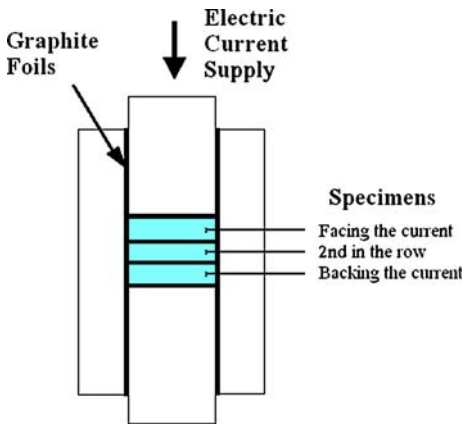

Fig. 1 Set-up of the three specimens in series with respect to the electric field and current

Results and discussion

The green density of the compacts showed large scatter with respect to the CIP pressure (Fig. 2). Nevertheless, the general trend of linear increase with the CIP pressure can be observed as shown by the leading lines in Fig. 2. Specimens at three different CIP pressures, which vary in their green density (filled circles in Fig. 2) were used for the porosity tests.

The intruded Hg volume versus pore radius in Fig. 3 revealed the pore size distribution in the fired specimens.

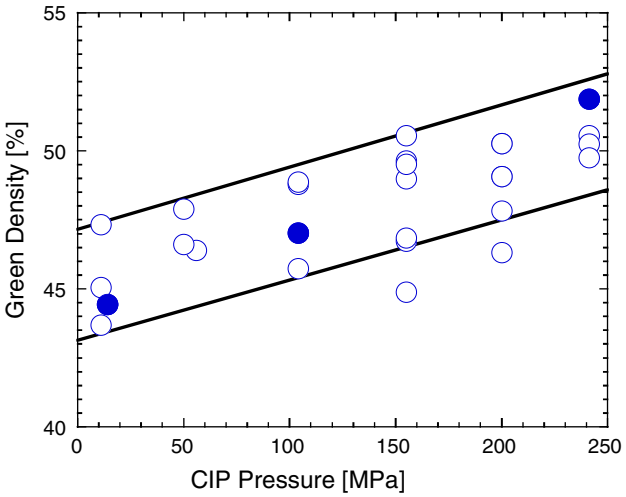

Fig. 2 Green density versus CIP pressure of YAG nano-powder compacts. The filled circles represent the specimens used for porosimetry

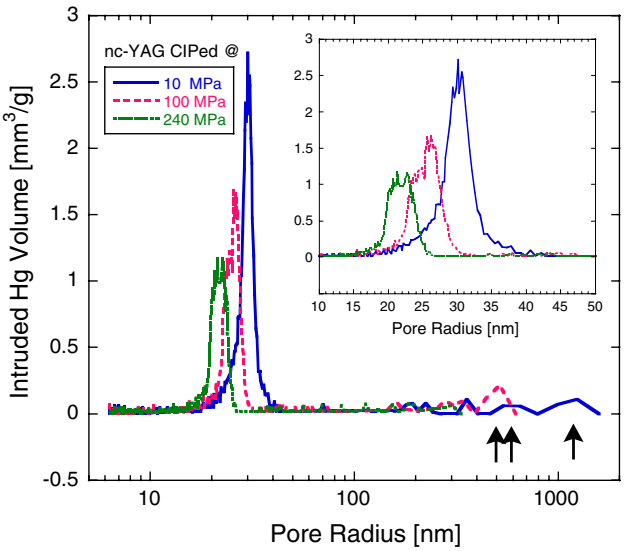

Fig. 3 Intruded Hg volume exhibit nanometric, micrometer (single arrow) and sub-micrometer size pores (double arrow) in CIPed nc-YAG. The average nanometric pore size between 20 and 30 nm decreases with the increase in the CIP pressure (insert)

The main pore volume is related to the many nanometric pores (see inset in Fig. 3) with average pore radius between 20 and 30 nm. Low fraction of this pore volume can be related to a fewer micrometer and sub-micrometer size pores. The larger pores diminished at higher CIP pressures; the average nanometric pore size and its volume decreased as well with the increase in the CIP pressure.

The final density after SPS versus the green density showed large scatter (Fig. 4). The final density generally increased with the increase in the green density. However, the final density was strongly associated with the specimen's location, with respect to the incoming electric current. The specimens facing the electric current (i.e., 1st in the row in Fig. 4) exhibited higher densities than those located as second or third (i.e., backing the electric current) in the row. The dashed line in Fig. 4 highlights this trend. Only one exception was found where specimen located at the center (i.e., 2nd in the row) with lowest green density (45%) exhibited very high final density (97.5%). The present findings may indicate that the specimens facing the current experienced the highest temperature, while those located as the third in the row experienced the lowest temperature in the same SPS run. It may have an important impact for re-evaluation of the symmetrical temperature gradients assumed along the disc/cylinder thickness in finite element analyses of the SPS process [18–22]. Once the direction of the electric field and the electrical conductivity of the specimen were considered, asymmetric electrical potential with higher values at the specimen surface facing the current flow were calculated [23]. This is in agreement with the present experimental findings.

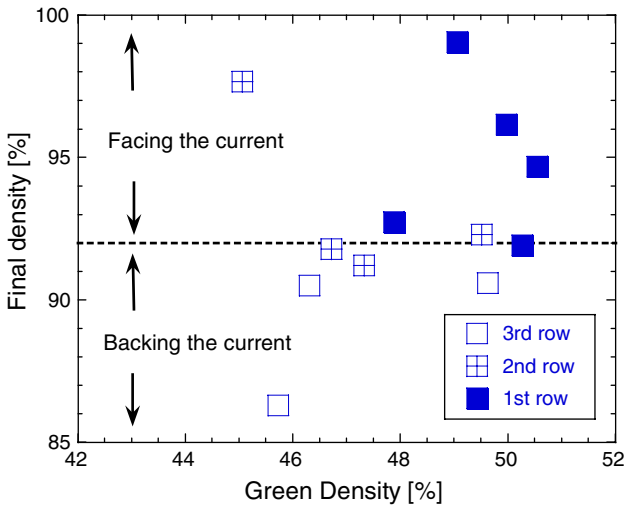

Fig. 4 Final density versus the green density. The specimens facing the electric current (1st in the row) exhibited higher final densities compared to those in the second row and third row (backing the current). The dashed line highlights the relative location of the specimens only

On the other hand, modeling the current distribution during SPS of non-conducting material (alumina) [8] indicated that axial displacement of the specimen changes its temperature; for a 3-mm thick specimen the axial temperature change was calculated as ~17 °C/mm. Using those calculations (Fig. 14 in Ref. 20) and the densities and dimensional changes measured in our nc-YAG specimens, the specimens facing (1st row) and backing (3rd row) the current may experience temperature gradient up to 62 °C (77 °C for the maximal displacement and 15 °C for the minimal displacement). Yet, it should be noted that the calculations in the above model were performed assuming the electrical resistivity of Alumina to be constant with temperature (i.e., 10^8 Ωm) [20]. Since electrical conductivity of most oxides increases exponentially with temperature, the expected temperature gradient between the externally located specimens (1st and 3rd row) should be far lower, because of the axial displacement during the SPS. Consequently, the observed differences in the final densities are too high to be related to the temperature change due to the specimen axial displacement. This is in agreement with the temperature gradient assumption along the die axis due to axially asymmetric current flow: specimens facing the current flow experienced higher SPS temperatures than those at the back.

Apparently the effect of green density on final densification of the specimens faded due to the limited range of the former (from 43 to 51%), combined with strong temperature effect caused by the relative location of the specimens. The temperature effect due to the current asymmetry along the pressing axis can further be supported following the average grain size and pore size in the studied specimens, as shown in Fig. 5. The average grain size and pore size were both in the nanometer size range. The average grain size increased with the increase in the final density (Fig. 5a) and was consistent with higher temperatures assumed for the specimens facing the electric current. Accordingly, the average pore size decreased with the increase in final density (Fig. 5b). The trajectories of the grain size and pore size versus final density were shown by arrows and followed the temperature increase as expected.

It is worth to note that both the grain size-density and the pore size-density trajectories span over a wide range of values, the boundaries of which are schematically drawn by the solid lines in Fig. 5a and b, respectively. Following this trend, two specimens facing the electric current (1st in the row) but showing distinctly different characteristics were compared, i.e., 94.5% dense specimen with 520 ± 20-nm grain size (CIPed at 150 MPa, green density 51%) versus denser specimen with 99.0% density and 340 ± 10-nm grain size (CIPed at 200 MPa, green density 49%) (Fig. 5a); these specimens were designated, respectively,

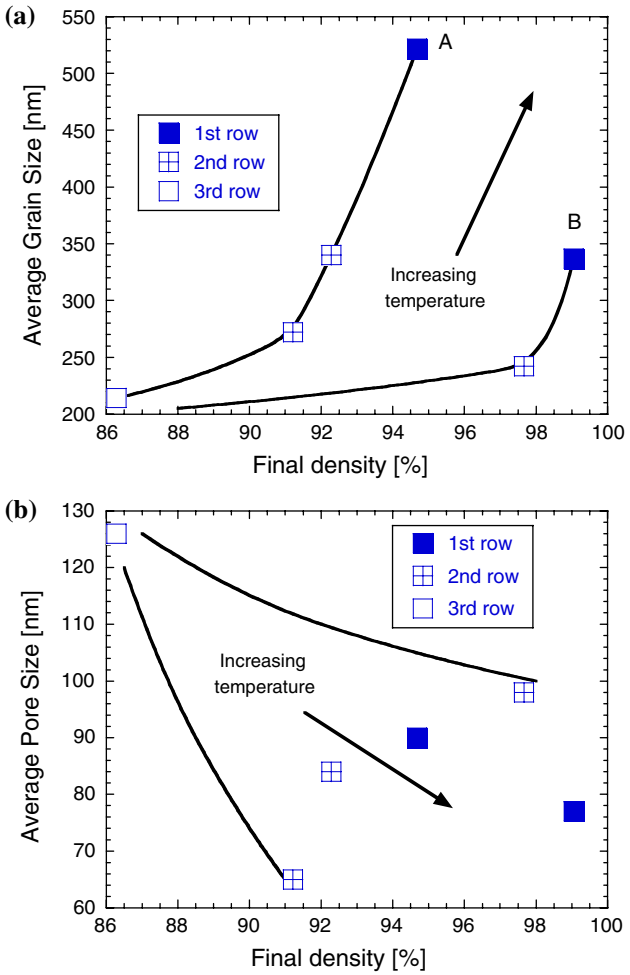

Fig. 5 **a** The increase in average grain size and **b** the decrease in average pore size with the increase in the final density, as shown by the trajectories (arrowed) that follow the temperature increase due to the specimen location in the row. The specimens 'A' and 'B' in (**a**) are discussed in the text

as 'A' and 'B' (denser) in Fig. 5a. The sintered microstructure of these two specimens in SEM significantly differed from each other. Specimen A was composed of grains that exceeded the micrometer size with large size distribution (Fig. 6a). Many isolated pores were found at both the grain boundaries and the grain interiors. In contrast, specimen B exhibited nanometric grain size below 650 nm and relatively narrow grain size distribution (Fig. 6b); no pores were observed within the grains. In order to compare the resultant microstructures with respect to their evolution during the SPS, the corresponding shrinkage curves versus temperature and duration are shown in Fig. 7. It was apparent that shrinkage took place during both the heating and at the SPS temperature. The total shrinkage during both the heating (3.6 vs. 3.8 mm) and at the SPS temperature (4.8 vs. 5.2) were comparable. The main difference was the immediate and time-independent initial shrinkage. It started in specimen A at 770 °C and 70 MPa, compared to 700 °C and 62 MPa in specimen B; the absolute shrinkage value was three times higher in specimen A compared with specimen B (3.2 vs. 1 mm). This difference is the main cause for the different density and grain size observed in these specimens, as will be shown below.

Recently, we thoroughly investigated the densification of the same nc-YAG powders by SPS [16, 17, 24]. It was shown that YAG exhibits very high yield stress above ~800 MPa at 1,500 °C [25]; it cannot be plastically deformed during the SPS under 90 MPa pressure. Nevertheless, the analysis of the grain growth kinetics and the microstructure evolution were in agreement with densification through grain rotation and sliding aided by surface viscous layer [16]. Following this mechanism, the immediate initial shrinkage in the studied specimens can be related to particles sliding over each other. On the one hand, the nano pore size and the micrometer pores were found to decrease in their size and volume fraction at increased CIP pressure. On the other hand, the decrease in the nanostructure features (particle and pore size) was shown to enhance the conditions for plasma formation, i.e., at lower input energy. These trends are consistent with the expectation for the lower immediate shrinkage observed in B specimen at lower temperature and pressure (Fig. 7b). However, the main shrinkage in specimen B is time

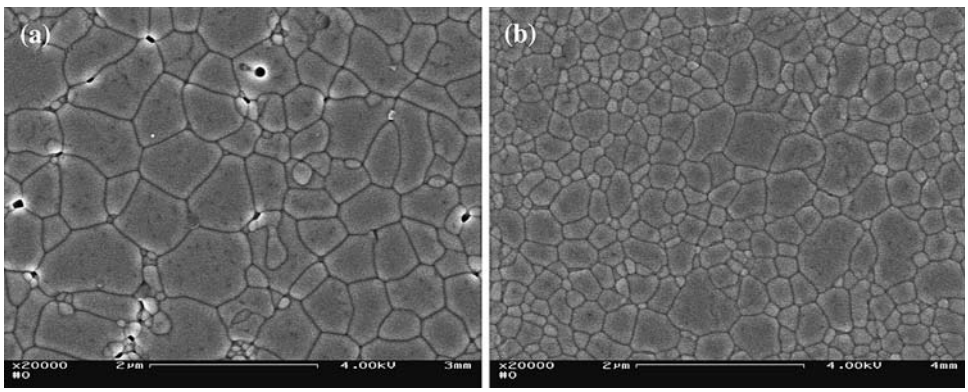

Fig. 6 SEM images showing the nc-YAG microstructure **a** 94.5% dense specimen with 520 ± 20 nm grain size, and **b** 99.0% dense specimen with 340 ± 10 nm grain size. The residual pores are visible in (**a**) but lack in (**b**)

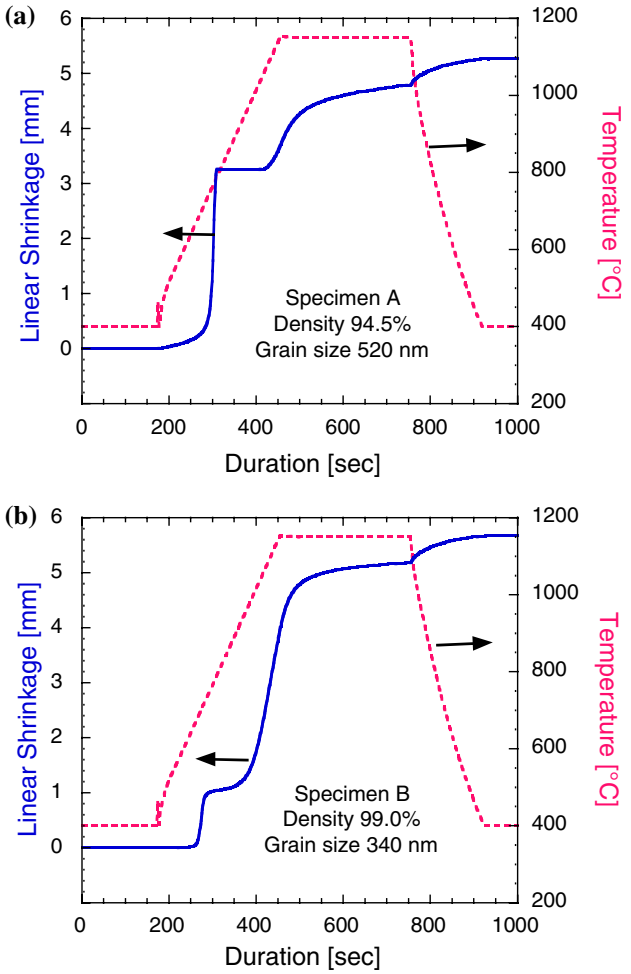

Fig. 7 Linear shrinkage versus temperature and duration during the SPS of nc-YAG CIPed at **a** 150 MPa, **b** 200 MPa

dependent during the heating and enables steady state sliding of the nano-particles; enough time is provided for the pores to be released from the evolving dense nano-grain clusters. In contrast, the higher immediate initial shrinkage in specimen A, which occurred at slightly higher temperature and pressure (Fig. 7a), is associated with dynamic compaction of the nano-particles. Consequently, the pores are trapped in the immediately densified nano-grain clusters, and their annealing out may necessitate lattice diffusion at high temperatures and for long durations, especially when the clusters undergo coarsening. In summary, the three fold higher rapid densification in specimen A at 800 °C provides locally dense regions that coarsen in contrast to slower densification rate and finer grains which evolve in specimen B. These processes are in agreement with the microstructures observed above. Similar effects and mechanisms were found and reported when changing the temperature at which the pressure is applied to the green compact [17].

Finally, a possible effect of the applied pressure gradient in the cluster of the three discs due to frictional forces should be evaluated. Graphite foils were used as high-temperature lubricants to separate between the specimens as well as between their surfaces and the die/punch surfaces (Fig. 1). For such compaction configuration with the height-to-diameter ratio of 1/3, the axial stress ratio for the bottom/top of alumina compact was 80% [26, 27]. Therefore, the applied pressure may be lower, i.e., 80 MPa in the specimens backing the current. In this respect, the effect of the applied pressure (50 and 100 MPa) on the final density of similar nc-YAG powders was investigated [28]. Application of these pressures for 3 min at 1,400 °C resulted in only 1% difference in the resultant densities. However, much larger density difference of 11% was recorded when the PS temperature was lowered only by 50–1,350 °C [28]. Recalling for our data, the reduced applied pressure of 80 MPa at 1,400 °C may not be responsible for the 10–15% difference density between the specimens facing and backing the current (Fig. 5). Nevertheless, the reduced applied pressure combined with the reduced SPS temperature may be responsible for the lower densities of the specimens backing the current.

Conclusions

The effect of CIP pressure and green density on the final density of nc-YAG densified by SPS was low to marginal, most probably because of the narrow range of the green density investigated. Apparently, efficient particle rearrangement takes place during the pressure application in SPS that screens the effect of the inherited green density from the CIP. This is in accordance with the rapid densification reported between 1,250 and 1,400 °C where enhanced particle surface diffusion exist [16].

Increase in the average grain size and decrease in the average pore size with increase in the final density showed the trajectories that followed the temperature increase. Effect of the electric current (field) direction on the specimen density (hence specimen temperature) was clearly observed, indicating the existence of asymmetric temperature gradient along the die axis. Specimens facing the incoming current exhibited higher densities than those backing the current flow. The contribution to the axial temperature gradient due to the electrically non-conductive specimen and the axial displacement are too insignificant to explain the observed effect.

Acknowledgements The financial supports by the Israel Ministry of Defense and Israel Ministry of Science are gratefully acknowledged. O. T.E.Z thanks M. Kats, M. Levin, and Dr. A. Berner from the Technion for the technical assistance, and Prof. N. Frage from BGU for providing the SPS facility.

References

1. Jiang D, Hulbert DM, Kuntz JD, Anselmi-Tamburini U, Mukherjee AK (2007) Mater Sci Eng A 463:89
2. Nygren M, Shen Z (2003) Solid State Sci 5:125
3. Dobedoe RS, West GD, Lewis MH (2003) Bull ECerS 1:19
4. Tokita M (2006) Am Ceram Soc Bull 85:32
5. Omori M (2000) Mater Sci Eng A 287:183
6. Liu W, Naka M (2003) Scripta Mater 48:1225
7. Vasylkiv O, Borodianska H, Sakka Y (2008) J Eur Ceram Soc 28:919
8. Munir ZA, Anselmi-Tamburini U, Ohyanagi M (2007) J Mater Sci 41:763. doi:10.1007/s10853-006-6555-2
9. Chaim R, Shen Z, Nygren M (2004) J Mater Res 19:2527
10. Anselmi-Tamburini U, Woolman JN, Munir ZA (2007) Adv Func Mater 17:3267
11. Bernard-Granger G, Guizard C (2007) Acta Mater 55:3493
12. Trunec M, Maca K, Shen Z (2008) Scripta Mater 59:23
13. Brook RJ (1969) J Am Ceram Soc 52:56
14. Wakai F, Akatsu T, Shinoda Y (2006) Acta Mater 54:793
15. Chaim R, Levin M, Shlayer A, Estournes C (2008) Adv Appl Ceramics 107:159
16. Chaim R, Marder-Jaeckel R, Shen JZ (2006) Mater Sci Eng A 429:74
17. Chaim R, Shen Z (2008) J Mater Sci 43:5023. doi:10.1007/s10853-008-2742-7
18. Yucheng W, Zhengyi F (2002) Mater Sci Eng B 90:34
19. Zavaliangos A, Zhang J, Krammer M, Groza JR (2004) Mater Sci Eng A 379:218
20. Anselmi-Tamburini U, Gennari S, Garay JE, Munir ZA (2005) Mater Sci Eng A 394:139
21. Vanmeensel K, Laptev A, Hennicke J, Vleugels J, Van der Biest O (2005) Acta Mater 53:4379
22. Wang X, Casolco SR, Xu G, Garay JE (2007) Acta Mater 55:3611
23. Matsugi K, Kuramoto H, Hatayama T, Yanagisawa O (2004) J Mater Proc Tech 146:274
24. Chaim R (2006) J Mater Sci 41:7862. doi:10.1007/s10853-006-0605-7
25. Chaim R (2007) Mater Sci Eng A 443:25
26. DiMilia RA, Reed JS (1983) J Am Ceram Soc 66:667
27. Reed JS (1995) Principles of ceramics processing, 2nd edn. Wiley, New York
28. Chaim R, Kalina M, Shen JZ (2007) J Eur Ceram Soc 27:3331